Circumstellar Dynamics at High Resolution
ASP Conference Series, Vol. 464
A. C. Carciofi and Th. Rivinius, eds.

Using Grids of High Resolution Synthetic Spectra in the Analysis of [WCE] Stars

G. R. Keller,[1] L. Bianchi,[2] J. E. Herald,[2] and W. J. Maciel[1]

[1]*Instituto de Astronomia, Geofísica e Ciências Atmosféricas, Universidade de São Paulo, Brazil*

[2]*Department of Physics and Astronomy, The Johns Hopkins University, Baltimore, Maryland, USA*

Abstract. Our grids of synthetic spectra cover the parameter regime of H-deficient central stars of planetary nebulae (CSPNe) of the [WC] and PG1159 types and were used to analyze UV and far-UV spectra of the hot [WCE] central stars of NGC 6905, NGC 5189 and Sand 3. The use of the grids enables systematic analysis of the observed spectra in order to constrain stellar parameters and facilitates line identification. The grids of synthetic spectra are available at http://dolomiti.pha.jhu.edu/planetarynebulae.html and will be augmented. The synthetic spectra from Keller et al. (2011), intended for [WC] stars with temperatures above 50 000 K, which are already on-line, have been recently updated to include the detailed flux calculation for wavelengths below 900 Å.

1. Introduction

Low and intermediate mass stars evolve from the Asymptotic Giant Branch (AGB) at an almost constant luminosity towards higher temperatures. These stars will, eventually, be hot enough to ionize the surrounding material, which was previously expelled by the AGB precursor, and become CSPNe. They are very hot objects, have high surface gravities and many of them present dense winds, whose features dominate the observed spectra. Their winds are likely driven by radiation pressure on spectral lines and, thus, inhomogeneous.

Weidmann & Gamen (2011) have found that about 30% of the CSPNe appear to be hydrogen-deficient. These H-poor CSPNe are commonly divided into [WC], showing strong C and He emission lines and PG1159 stars, positioned at the top of the WD cooling track and exhibiting absorption lines of highly ionized He, C and O, besides weak UV wind lines and very high terminal velocities of the wind.

2. The Grids

The grids of synthetic spectra presented in part in Keller et al. (2011) are intended to comprehensively cover the parameter space of hydrogen-deficient CSPNe. The combination of parameters chosen for each of the grid models approximately follows the evolutionary calculations of Miller Bertolami & Althaus (2006). The stellar parameters L, $R_\star$, $T_\star$, $\log g$, $M_\star$, v_∞ and $\dot{M}$ (and also the transformed radius, defined as

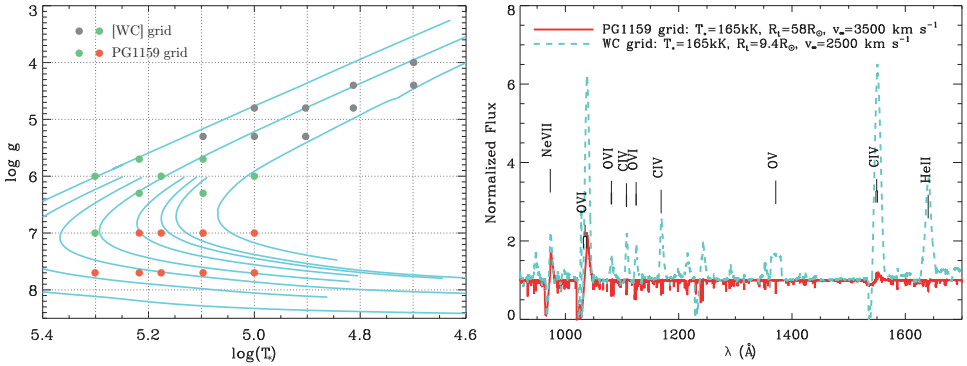

Figure 1. *Left panel:* the [WC] (gray and green dots) and PG1159 (green and orange dots) grids of synthetic spectra are shown on the $\log(T_\star) \times \log(g)$ diagram, along with evolutionary calculations from Miller Bertolami & Althaus (2006), in blue. *Right panel:* comparison between similar temperature synthetic spectra from the PG1159 and the [WC] grids. The PG1159 models have fainter winds that reach higher terminal velocities than the ones from the [WC] grid models.

$R_t = R_\star[(v_\infty/2500 \text{ km s}^{-1})/(\dot{M}/10^{-4} \text{ M}_\odot \text{ yr}^{-1})]^{2/3}$) of the grid models are inside the range of values found in the literature for these stars, taking into account that our models assume a clumped wind whereas some mass-loss rates were derived in the literature assuming a smooth wind. The models include many ionic species previously neglected and were calculated with the non-LTE stellar atmosphere code CMFGEN (Hillier & Miller 1998), which accounts for spherically symmetric stationary expanding atmospheres, line blanketing and wind clumping.

The grid of synthetic spectra appropriate for the analysis of [WC] stars with temperatures above 50 000 K is already available on-line at http://dolomiti.pha.jhu.edu/planetarynebulae.html. There, the users have access to the synthetic spectra and related documentation, along with plots comparing different models. The PG1159 grid of models will follow soon. The left panel of Fig. 1 shows the two grids on the $\log(T_\star) \times \log(g)$ diagram. Each dot shown corresponds to a group of models differing only in v_∞ and $\dot{M}$, such that the [WC] and the PG1159 grids so far add up to a total of 199 and 160 models, respectively.

Figure 2 shows the ionization fractions of helium, carbon, oxygen and neon in models with temperatures of 165 000 K and 125 000 K from the [WC] and PG1159 grids. The winds of the [WC] grid models show stratified neon and oxygen radial ionization profiles, different from the ionization fractions seen in the PG1159 models. The [WC] models also have denser winds with lower terminal velocities than those adopted on the PG1159 grid models, as can, for example, be seen on the right panel of Fig. 1, where we show a comparison between two synthetic spectra from models of similar temperature (also shown in Fig. 2), one from the PG1159 grid and the other from the [WC] one.

For the [WC] grid, we have recently added to the website the detailed flux for wavelengths below 900 Å, which is the energy regime responsible for the ionization of the nebulae (see, for example, Morisset & Georgiev 2009). Examples of such spectra are shown in Fig. 3.

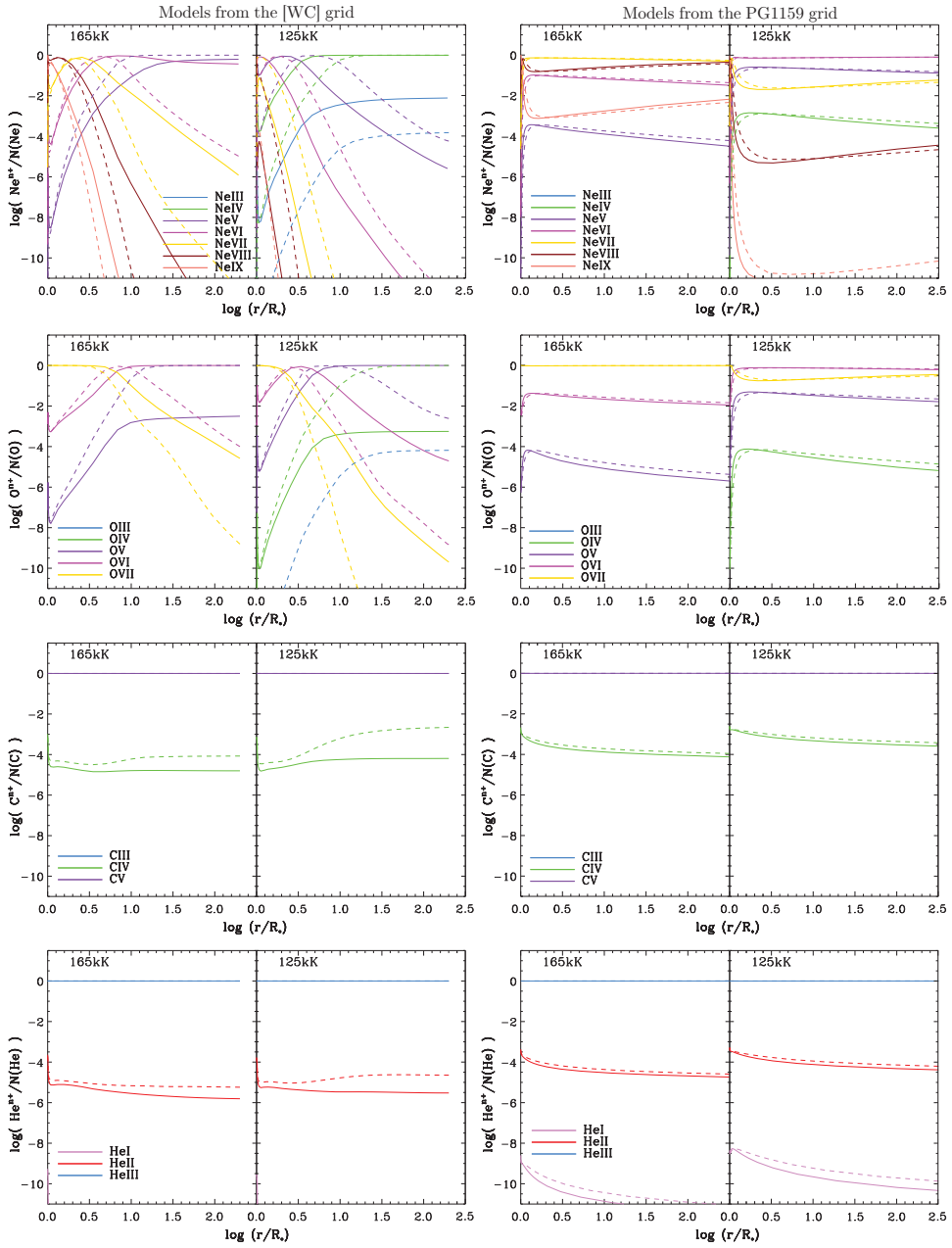

Figure 2. Ionization fractions of helium, carbon, oxygen and neon in models with temperatures of 165 000 K and 125 000 K from the [WC] and PG1159 grids. *Left panels:* models are from the [WC] grid. For $T_\star$ = 125 kK, continuous lines represent models with R_t = 18.2 $R_\odot$ and the dashed ones, R_t = 8.7 $R_\odot$. For $T_\star$ = 165 kK, continuous lines represent models with R_t = 9.4 $R_\odot$ and the dashed ones, R_t = 4.5 $R_\odot$. All [WC] models shown have v_∞ = 2500 km s^{-1}. *Right panels:* models are from the PG1159 grid. The continuous lines represent models with R_t = 90 $R_\odot$ and the dashed ones, R_t = 58 $R_\odot$. All PG1159 models shown have v_∞ = 3500 km s^{-1}.

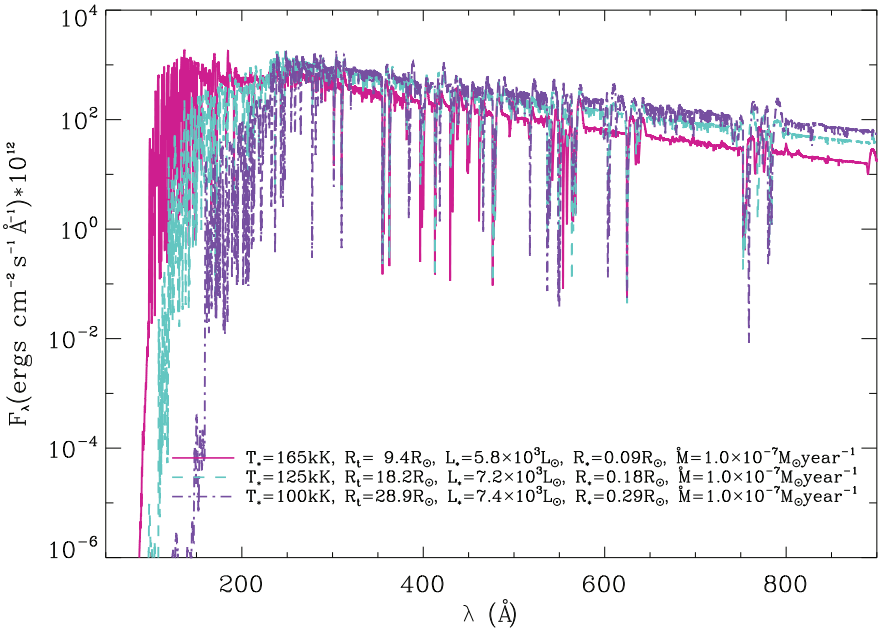

Figure 3. Detailed flux for wavelengths below 900 Å are now available for the [WC] grid models, calculated for a distance of 1 kpc. The sample spectra shown here result from models of similar mass-loss rates and terminal velocities of the wind (v_∞ = 2500 km s^{-1}), but different temperatures, stellar radii and luminosities.

3. Analysis of [WCE] Stars

We used the [WC] grid to constrain the temperature and transformed radius of three hot [WCE] central stars: NGC 6905, NGC 5189 and Sand 3. The combined FUSE, HST/STIS and IUE spectra cover the wavelength range between 905 and 3200 Å, with resolution varying from ∼0.06 Å (FUSE) to ∼7 Å (IUE), and were obtained from MAST. The procedure adopted by us is described in detail on Keller et al. (2011) for the central star of NGC 6905. Once the terminal velocity of the wind is measured from the blue edge of the C IV 1548.2 Å P Cygni profile, the grid model spectra of the appropriate v_∞ are compared to the observations, such as illustrated in Figs 4, 5 and 6, for the central stars of NGC 6905, Sand 3, and NGC 5189, respectively. For each temperature value available, there are many transformed radius values to choose from in the grid and R_t can be constrained by fitting the strong He II 1640.4 Å emission line, which is the best diagnostic of transformed radius available in the spectra of [WCE] CSPNe, since it shows little sensitivity to temperature and helium abundance in this parameter regime. Constraining temperature usually requires observations of spectral lines from different ionization stages of the same element, but these are scarce in the spectra of [WCE] CSPNe and the strengths of the two available O V lines were found to be quite dependent on the inclusion of further sources of opacity in the calculations (Keller et al. 2011, 2012). Thus, the existence or absence of features in the spectra due to ions of different ionization potentials, along with the general appearance of the spectral lines is

also used as a temperature diagnostic. Having constrained temperature and transformed radius, we then proceed by considering other parameters not extensively explored by the grid, such as turbulence velocity, abundance patterns and additional elements. The main stellar parameters of our best fitting models for each object studied are shown on Table 1. Figure 7 shows samples of the final fits obtained. The complete analysis, also varying parameters not covered by the model grids, will be presented in detail in Keller et al. (in prep.).

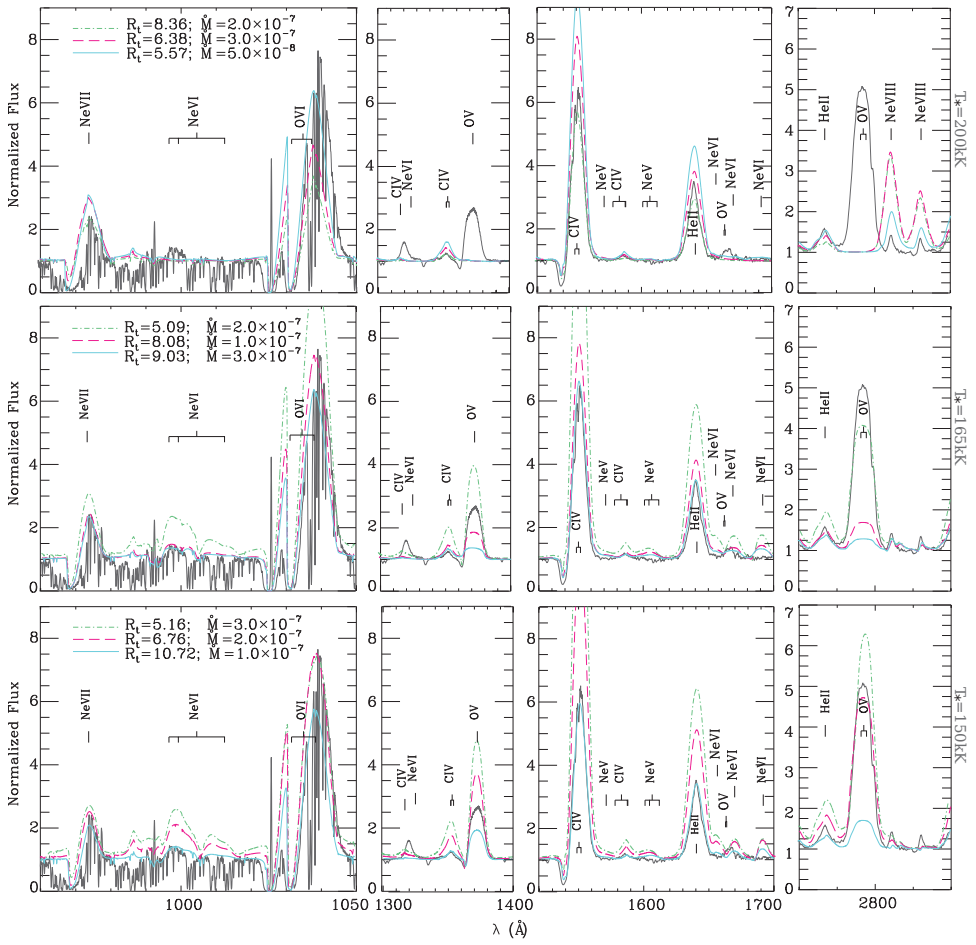

Figure 4. UV and far-UV observed spectra (continuous black line) of the central star of NGC 6905 and models (colored lines) with $T_\star$ = 150, 165 and 200 kK and various values of transformed radius (transformed radii and mass-loss rates are given in units of $R_\odot$ and $M_\odot$ yr^{-1}, respectively). All the models shown have v_∞ = 2000 km s^{-1}.

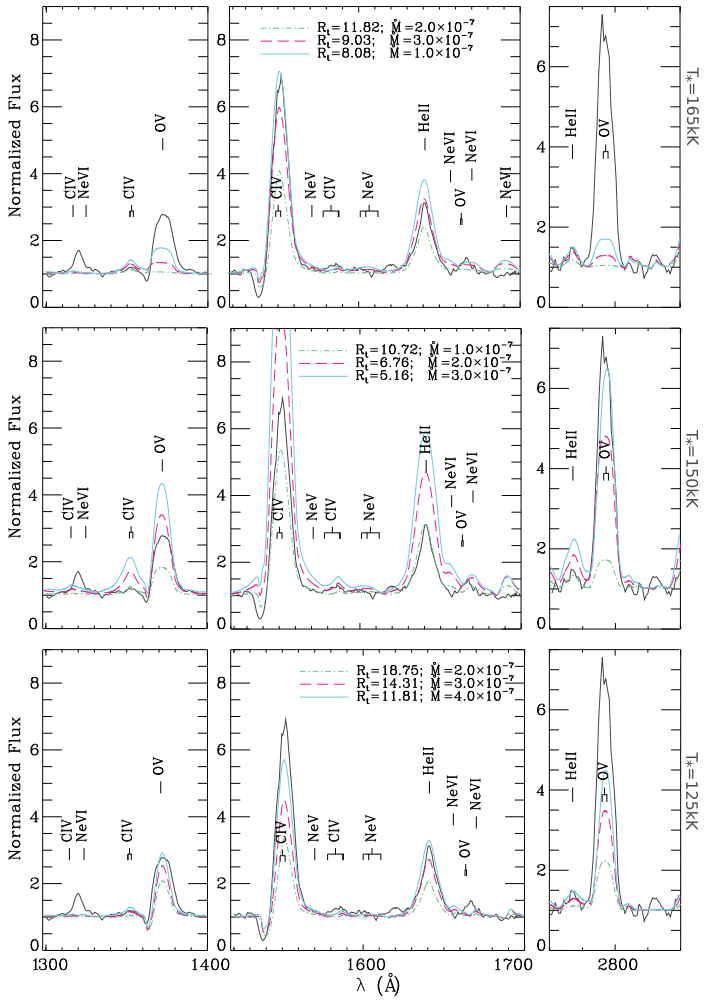

Figure 5. UV observed spectra (continuous black line) of the central star of Sand 3 and models (colored lines) with $T_\star$ = 125, 150 and 165 kK and various values of transformed radius (transformed radii and mass-loss rates are given in units of $R_\odot$ and $M_\odot$ yr^{-1}, respectively). All the models shown have v_∞ = 2000 km s^{-1}.

Table 1. Main stellar parameters of our best fitting models. $T_\star$ is the temperature at an optical depth of 20, $X_{\rm He}$, $X_{\rm C}$, $X_{\rm O}$ and $X_{\rm Ne}$ are He, C, O and Ne mass fractions.

Object	$T_\star$ [kK]	R_t [$R_\odot$]	v_∞ [km s^{-1}]	X_{He}	X_C	X_O	X_{Ne}
NGC 6905	150	10.7	2000	0.44	0.45	0.08	0.02
NGC 5189	165	10.5	2500	0.58	0.25	0.12	0.04
Sand 3	150	9.3	2000	0.28	0.55	0.08	0.02

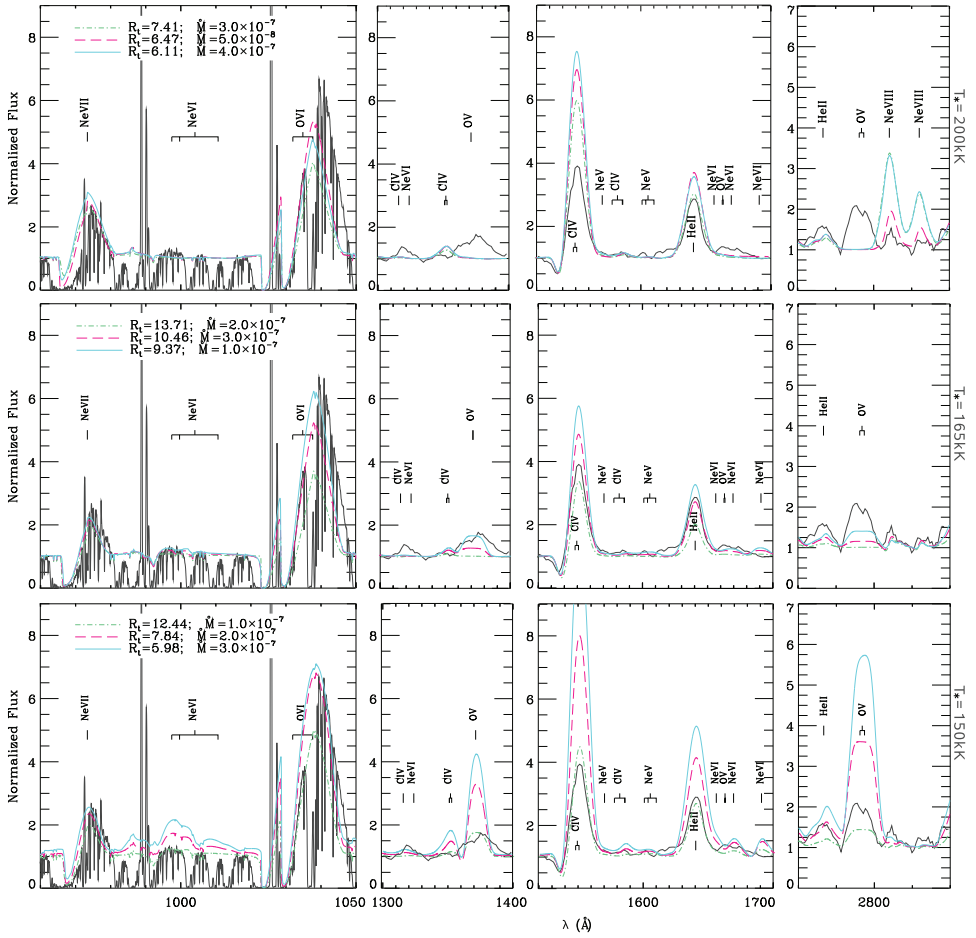

Figure 6. UV and far-UV observed spectra (continuous black line) of the central star of NGC 5189 and models (colored lines) with $T_\star$ = 150, 165 and 200 kK and various values of transformed radius (transformed radii and mass-loss rates are given in units of $R_\odot$ and $M_\odot$ yr^{-1}, respectively). All the models shown have v_∞ = 2500 km s^{-1}.

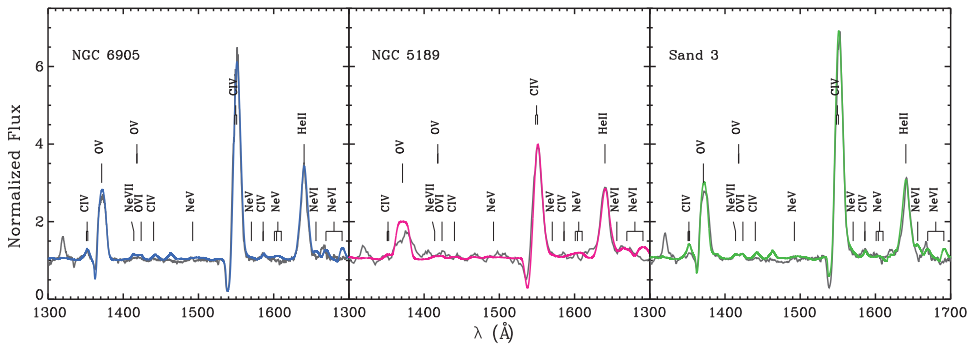

Figure 7. Observed spectra (black continuous lines) of the central stars of NGC 6905, NGC 5189 and Sand 3 in the region between 1300 and 1700 Å shown with our best-fitting models (colored lines).

Acknowledgments. GRK acknowledges support from the grants CAPES-0370-09-6 and Fapesp-06/58240-3. The data presented here were obtained from MAST.

References

Hillier, D. J., & Miller, D. L. 1998, ApJ, 496, 407
Keller, G. R., Bianchi, L., Herald, J. E., et al. 2012, in Planetary Nebulae: An Eye to the Future, edited by A. Manchado, L. Stanghellini, & D. Schönberner, vol. 283 of IAU Symposium. In press.
Keller, G. R., Herald, J. E., Bianchi, L., et al. 2011, MNRAS, 418, 705
Miller Bertolami, M. M., & Althaus, L. G. 2006, A&A, 454, 845
Morisset, C., & Georgiev, L. 2009, A&A, 507, 1517
Weidmann, W. A., & Gamen, R. 2011, A&A, 526, A6

Discussion

Sundqvist: There are some studies (e.g. Kudritzki et al. 2006) that indicate that at least some of the winds from CSPNe are strongly clumped, which will affect your diagnostics. So I was just wondering whether this is something you have considered.

Keller: CMFGEN accounts for clumping using an exponential law, such that the wind is assumed smooth until a certain wind velocity is achieved. Beyond that, the degree of clumping increases outwards until the clumping filling factor reaches a terminal value, which we assumed to be 0.1. We, however, are under the impression that a less clumped wind could give us better fits to the observations. The observed far-UV P Cygni profiles are generally too strong compared to our best fitting models. By decreasing the amount of clumping in the wind, we should be able to fit the emission lines using higher mass-loss rates, which should increase the strength of the synthetic P Cygni profiles (in comparison to what is predicted by the more clumped models) and improve their fit. This will be our next step in this work.

Oudmaijer: How do the iron (or other metallicity tracers) values in the nebulae compare to those you determined in the wind?

Keller: For the central stars of NGC 6905 and NGC 5189, we found the iron mass fractions to be below 0.3 times the solar value. Previous works by different authors have also reported sub-solar iron abundances of this order for [WC] type CSPNe. For PG1159 stars, on the other hand, recent papers by Klaus Werner report solar iron abundances. Iron is a refractory element and the low abundances measured in the nebular gas phase compared to solar are interpreted as depletion into dust grains. We have also modeled a far-UV argon line and found that strong argon overabundances are able to improve the fit to the observed line profile. These results are however conflicting, since the Ar abundances, as measured in PNe, are thought to remain at the levels in which the progenitor stars formed, but we suspect our fit of the argon line to be affected by the clumping filling factor we adopted.

Baade: How did you identify the most promising diagnostics? By eye or something like principal component analysis?

Keller: By eye, but it is in our plans to apply PCA to the grids and have quantitative indicators.